scientific reports

Check for updates

OPEN

Liver dysfunction triggers early Alzheimer's pathology in an adult rat model of chronic liver disease

O. Braissant[1], V. A. McLin[2], D. Sessa[2] & K. Pierzchala[3,4]✉

Emerging evidence links liver dysfunction to Alzheimer's disease (AD), though few studies have investigated this connection. While cirrhosis is associated with cognitive impairment, its underlying mechanisms remain poorly understood. This study aimed to assess the presence of central nervous system (CNS) markers of Alzheimer's disease in a rat model of chronic liver disease. Standard histochemical techniques were employed, including Congo red staining for amyloid-β (Aβ) and Gallyas silver staining for tau pathology. Immunohistochemistry was used to evaluate changes in aquaporin (Aqp1, Aqp4, Aqp9) expression and astrocytic glial fibrillary acidic protein (GFAP) levels. Furthermore, blood concentrations of neurodegeneration markers, neurofilament light chain (NfL), Aβ, phosphorylated tau (p-tau), total tau (t-tau), GFAP, and myelin oligodendrocyte glycoprotein (MOG), along with bile acids, were quantified and compared between BDL and SHAM control groups to investigate potential systemic correlates of CNS pathology. CNS analysis revealed the presence of intracellular amyloid-β (iAβ) and abnormal tau aggregates (pre-tangle/tangle stages), consistent with early AD pathology. Additionally, alterations in aquaporin water channels and astrocytic GFAP expression were observed. Peripheral blood analysis showed significant changes in neurodegeneration markers (NfL, Aβ, p-tau, t-tau, GFAP, MOG) and bile acid profiles, reinforcing the systemic nature of neuroinflammatory processes in liver disease. Our findings emphasize liver failure as a significant factor in cognitive decline and increased AD risk. The study advocates for incorporating liver function screening into the diagnostic workup of patients with dementia.

Keywords Chronic liver disease, Alzheimer's disease, Neurodegeneration, Neurometabolism, Neurofilaments, Amyloid-β, Tau-bodies

Abbreviations

Aβ	Amyloid beta
Aqp	Aquaporin
ALT/GPT	Alanine aminotransferase
AST/GOT	Aspartate aminotransferase
BBB	Blood-brain barrier
BDL	Bile duct ligation
CAA	Cerebral amyloid angiopathy
CLD	Chronic liver disease
CNS	Central nervous system
GFAP	Glial fibrillary acidic protein
MOG	Myelin oligodendrocyte glycoprotein
NfL	Neurofilament light chain
IHC	Immunohistochemistry
type C HE	Type C hepatic encephalopathy

Every year, over 10 million new cases of dementia are diagnosed worldwide[1]. Alzheimer's disease (AD) accounts for 60–80% of these cases and primarily manifests as memory loss and cognitive decline. Additionally,

[1]Service of Clinical Chemistry, Lausanne University Hospital and University of Lausanne, Lausanne, Switzerland. [2]Department of Pediatrics, Gynecology and Obstetrics, Swiss Pediatric Liver Center, University Hospitals Geneva and University of Geneva, Geneva, Switzerland. [3]CIBM Center for Biomedical Imaging, EPFL AVP CP CIBM-AIT, CH F1 602, Station 6, 1015 Lausanne, Switzerland. [4]CIBM-PCI EPFL Metabolic Imaging Section, Ecole Polytechnique Fédérale de Lausanne, Lausanne, Switzerland. ✉email: katarzyna.pierzchala@epfl.ch

approximately 5–10% of individuals develop vascular dementia[2]. The brain changes associated with AD are believed to begin 20 years or more before symptoms, involving glucose hypometabolism, amyloid β (Aβ) accumulation, tau protein hyperphosphorylation (resulting in neurofibrillary tangles formation (NFTs)), neurodegeneration and neuroinflammation[3].

Growing evidence highlights liver role in AD pathogenesis. Few studies have explored this link[4,5], some suggesting an impairment of Aβ clearance by liver[6]. Studies confirm association between cirrhosis and cognitive impairment[7,8], suggesting liver disfunction as an important risk factor causing cognitive decline[7,8]. There is increasing interest in the role of liver dysfunction as a potential contributor to Aβ deposits[4,9].

Despite progress in understanding the mechanisms of type C hepatic encephalopathy (HE), a consequence of chronic liver disease (CLD) affecting up to 80% of patients, the impact on cognition and dementia risk remains poorly defined[10–12]. Cognitive dysfunction in type C HE involves attention and memory deficits[13]. This raises the question of whether these neurocognitive impairments are linked to AD—an area that remains underexplored. The association between hyperammonemia and cognitive decline has been discussed in the literature since the early 1980s[14]. At that time, studies showed that Alzheimer's patients were unable to maintain ammonia levels within the normal range[14]. Ammonia, a recognized neurotoxin, may contribute to AD progression. Unfortunately, the role of the gut-liver-brain axis in neuropathology has only recently regained scientific attention, highlighting the importance of liver health for central nervous system (CNS) function[4,8,15].

It is also well established that neurodegenerative diseases cause metabolic and cellular abnormalities in the brain. We have previously demonstrated neurometabolic changes in BDL rat model (bile duct ligation (BDL))[16] of CLD including increased glutamine levels and alterations in neurotransmitters, osmolytes, antioxidants, and glucose metabolism[11,17,18]. These alterations were accompanied by increased oxidative stress (OS) and inflammation, both systemic and within the CNS, notably characterized by a significant accumulation of IL-6 in the brain, a pleiotropic pro-inflammatory cytokine [10,12]. Furthermore, increased IL-6 concentrations observed in the brains of BDL rats have been associated with aging processes, central nervous system injury responses, compromised blood–brain barrier integrity, and deterioration of memory and cognitive performance[10]. Moreover, our recent studies in BDL rats revealed significant morphological activation-related changes in astrocytes and microglia, along with morphological alterations in neurons[11,17,19].

To the best of our knowledge, this is the first longitudinal study analyzing the Alzheimer's disease-related features in a BDL rat model, an established model of CLD (Fig. 1).

Our integrated approach uniquely combines the experimental advantages of CNS histochemistry, immunohistochemistry, and UV–Vis spectroscopy of immunolabeled brain sections, alongside the detection of blood-based (systemic) neurodegeneration markers (neurofilament light chain (NfL), Aβ, phosphorylated tau (p-tau), total tau (t-tau), glial fibrillary acidic protein (GFAP), and myelin oligodendrocyte glycoprotein (MOG)), provides a comprehensive view of disease progression from peripheral to central levels.

Results

Chronic liver disease induction

Blood biochemistry confirmed chronic liver disease (CLD). In line with our previous findings[11,12,19], we observed an early (2 weeks post-BDL) increase in blood ammonia, plasma bilirubin, and liver function markers, such as aspartate aminotransferase (AST/GOT) and alanine aminotransferase (ALT/GPT) (Fig. 2). Additionally, a significant decline in blood glucose levels was noted as the disease progressed (Fig. 2).

Histology

Histochemistry: signatures of Alzheimer disease in CLD

At 4-weeks post BDL surgery, Congo red staining revealed intracellular Aβ accumulation in several brain regions of BDL rats, with the accumulation increasing as the disease progressed in frontal cortex (Fr), frontoparietal cortex—motor area (FrPaM), cingulate gyrus (Cg), hippocampus (Hipp), striatum (Str), thalamus (Thal), midbrain colliculus (Col), Pons, medulla oblongata (MO), cerebellum (Cer), olfactory tubercle (Olf) (Fig. 3A). In addition, there was a strong accumulation of Aβ in the region of neuronal nuclei and diffuse Aβ in the cytoplasm (Fig. 3A, Fig. S1). In addition, abnormalities of the arterial vessel wall suggested (Fig. 3B, Fig. S1) cerebral amyloid angiopathy (CAA).

Gallyas staining revealed abnormal tau-bodies in the pre-tangle and neurofibrillary tangles (NFTs) status in the frontal cortex (Fr), frontoparietal cortex—motor area (FrPaM), cerebellum (Cer), olfactory tubercle (Olf) and piriform cortex (Pir) (Fig. 4).

Immunohistochemistry and immunofluorescence (UV–Vis spectroscopy)

Aqp1, Aqp4, Aqp9 and GFAP staining analysis was performed in the hippocampus and cerebellum. Immunolabeling followed by UV–Vis spectroscopy of immunofluorescence revealed a statistically significant fluorescence signal intensity alterations in all the labeled proteins already at 4-weeks post-BDL.

Aqp1 immunoreactivity was observed in the hippocampal astrocytes, granular neurons and vessels of SHAM rat's (Fig. 5A). In the cerebellum of SHAM rats strong Aqp1 expression was seen in the soma of Purkinje cells, and was weaker in the granular cells layer and astrocytes (Fig. 5B). Increased expression of Aqp1 was observed in both brain regions as disease progressed. In the hippocampus, Aqp1 channels were localized to granule cells as well as to astrocytes, specifically within the soma and processes of the latter (Fig. 5A). Quantitative analysis of Aqp1 immunofluorescence signals showed significant increase already at week 4 post-BDL. The immunofluorescence of Aqp1 increased significantly in the hippocampus (+32%, $p < 0.05$) and cerebellum (+66%, $p < 0.01$) as early as week 4 post-BDL, and continued to rise until week 8 (Fig. 5A,B).

In the SHAM rats the Aqp4 immunostaining was mostly detected around the hippocampal (Fig. 5C) and cerebellar microvessels (Fig. 5D). With the disease progression Aqp4 microvessels immunolabeling decreased

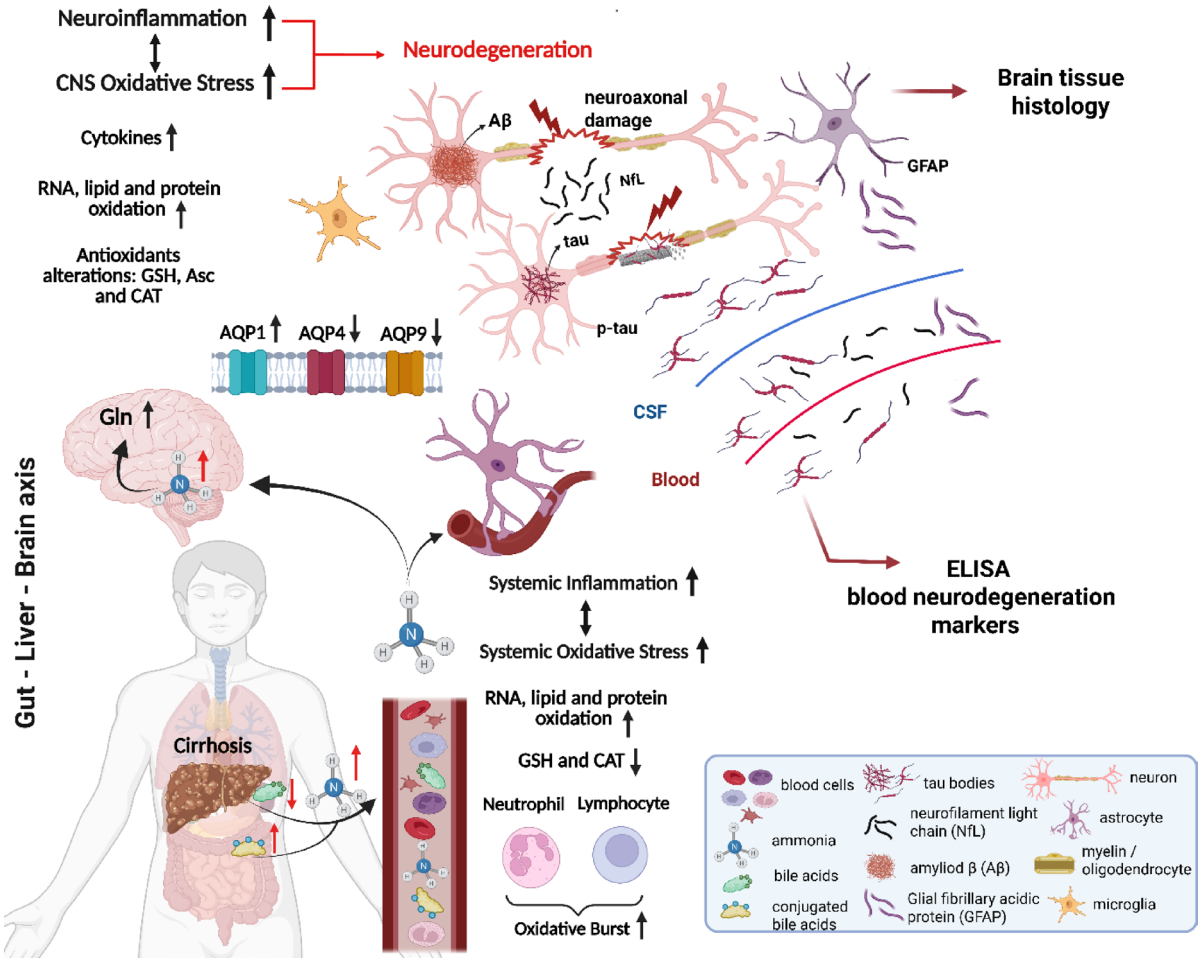

Fig. 1. Overview of existing knowledge and study insights. Created with BioRender.com.

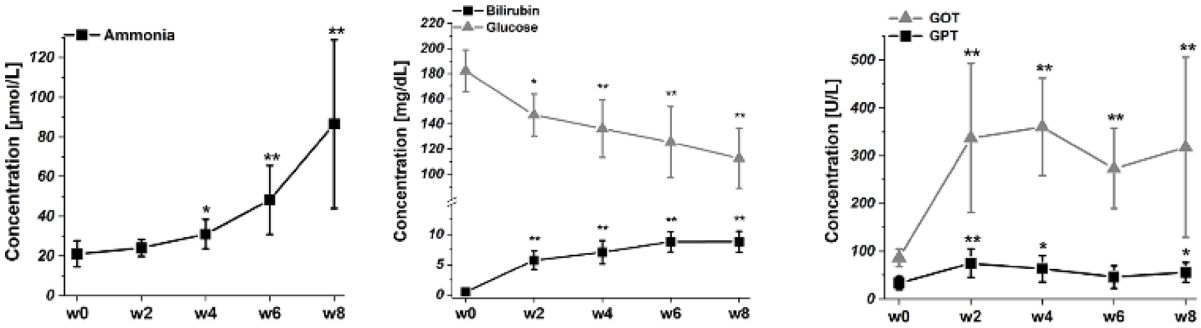

Fig. 2. Longitudinal changes in blood ammonia, total plasma bilirubin, glucose, GOT and GPT induced by the bile duct ligation. Bilirubin was undetectable before BDL. Data are presented as mean ± SD and statistical significance between week 0 and weeks 2–8: $^{*}p < 0.05$, $^{**}p < 0.01$ (One-way Anova with post-hoc Tukey HSD).

significantly in both the hippocampus and cerebellum. At week 4 post-BDL Aqp4 labeling was more visible in the astrocytes processes and endfeet near the blood vessels in the hippocampus (Fig. 5C) but not in the cerebellum. Quantitative analysis revealed a significant decrease in Aqp4 immunofluorescence intensity starting at week 4 post-BDL, with reductions of -32% in the hippocampus ($p < 0.01$) and −33% in the cerebellum ($p < 0.01$) (Fig. 5C,D).

Aqp9 immunoreactivity was seen in astrocytic somata and processes of the hippocampus and cerebellum of SHAM rats (Fig. 5E,F). In addition, in the cerebellum of the SHAM rat's Aqp9 immunolabeling was also present in the Purkinje cells, both in soma and in the dendritic trees. The quantitative analysis of Aqp9 immunofluorescence

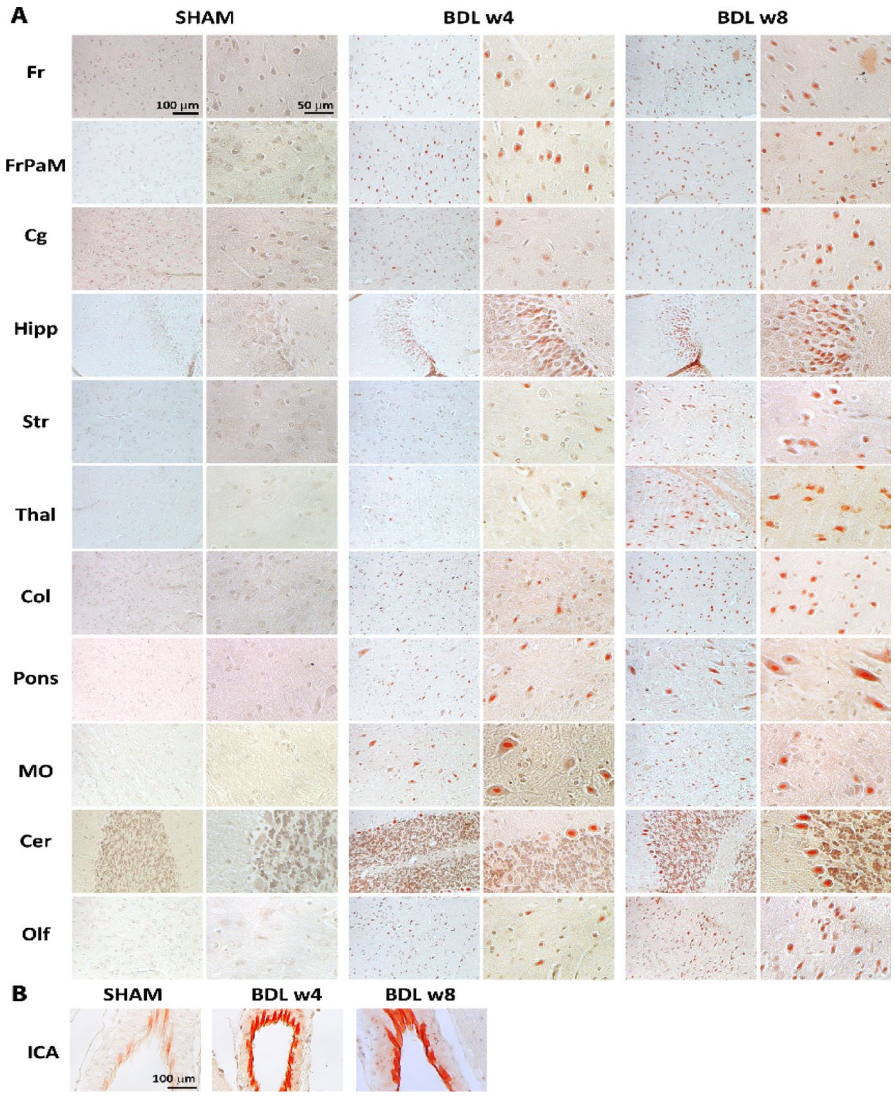

Fig. 3. **Amyloid β accumulation in the brain visualized with Congo red histochemical stain.** Representative microphotographs of the BDL rats' brain and age-matched SHAM controls. Initial intraneuronal Aβ deposits (red) are detectable at 4-weeks post-BDL, and increase with disease progression. The BDL revealed positive signal of intracellular Aβ accumulation in frontal cortex (Fr), frontoparietal cortex—motor area (FrPaM), cingulate gyrus (Cg), hippocampus (Hipp), striatum (Str), thalamus (Thal), midbrain colliculus (Col), Pons, medulla oblongata (MO), cerebellum (Cer), olfactory tubercle (Olf) (**A**), and also deposits in brain arteries, here the internal common carotid artery (ICA) (**B**) indicating cerebral amyloid angiopathy.

signals in the hippocampus revealed a non-significant signal increase at week 4 post-BDL (+9%) followed by a significant decrease at week 8 (−20%, $p<0.01$). In the cerebellum the Aqp9 immunolabeling of Purkinje cells was almost lost and the immunofluorescence signals decreased starting at week 4 post BDL (−33%, $p<0.01$) (Fig. 5E,F).

As previously reported[19], GFAP staining revealed a reactive astrocytic response (astrocytosis), characterized by a visible increase in GFAP+ cells at week 4 post-BDL, followed by a reduction in astrocytosis at week 8 compared to week 4 post-BDL (Fig. 5A–E). These findings are consistent with the quantitative analyses of GFAP fluorescence intensity in the hippocampus and cerebellum (Fig. 5A,B), which show an increased GFAP signal in BDL rats at week 4 (hippocampus + 26% ($p<0.001$), cerebellum + 24% ($p<0.01$)) and an overall decrease at week 8 vs. week 4 (hippocampus − 55% ($p<0.001$), cerebellum − 23% ($p<0.01$)) (Fig. 5A,B).

Determination of neurodegeneration markers in blood

NfL Neurofilament light chain concentrations were measured in plasma of BDL and SHAM rats since its increase is related to axonal damage and is associated to neuroinflammation[20]. The BDL group exhibited significantly higher levels of NfL (+137%, $p<0.05$) compared to the SHAM group as of 4 weeks post BDL surgery and continued to increase until the week 8 (+305%, $p<0.001$) (Fig. 6A).

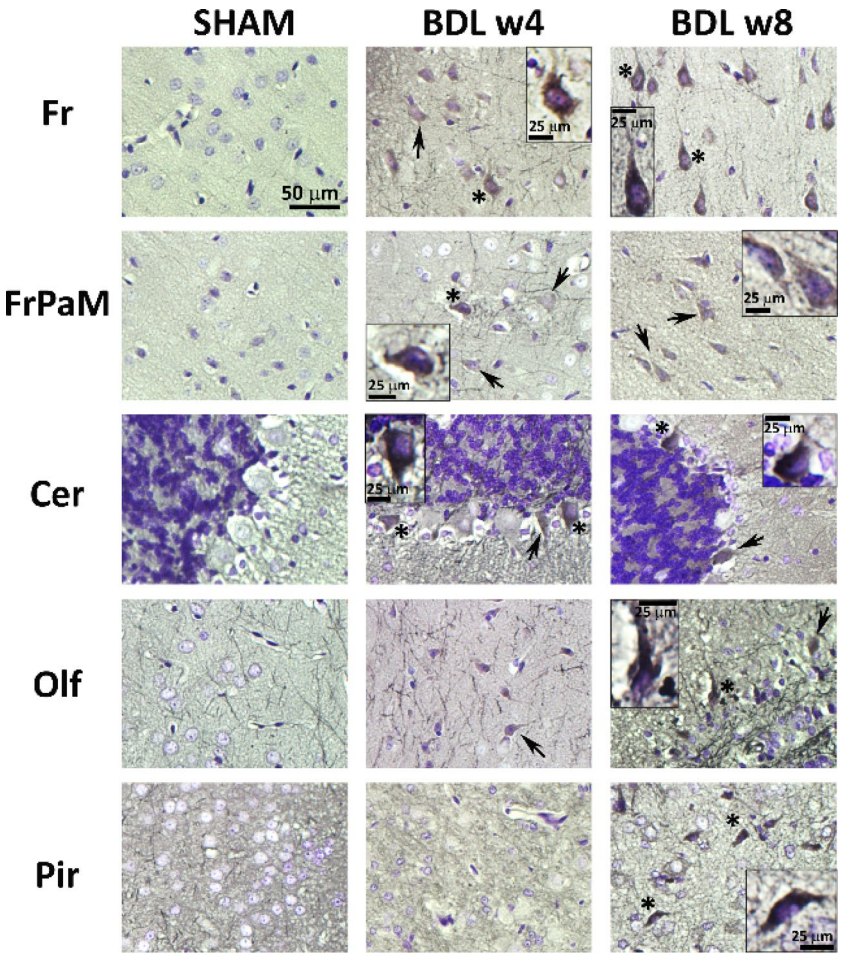

Fig. 4. **Representative micrographs of Gallyas silver stain** of the BDL rat's brain and age-matched SHAM controls revealed accumulation of abnormal tau-protein in the pre-tangle status (arrow) and more advanced forms of NFTs (asterisk) in frontal cortex (Fr), frontoparietal cortex—motor area (FrPaM), cerebellum (Cer), olfactory tubercle (Olf) and piriform cortex (Pir).

Tau-bodies Concentrations of tau protein, the axonal cytoskeleton-stabilizing element[21], was assessed in plasma samples of BDL and SHAM rats. The mean levels of tau proteins were significantly elevated in BDL group at week 8 compared to the SHAM rats (t-tau + 713% ($p < 0.001$) and p-tau + 339% ($p < 0.01$)). Reduced p/t-tau ratio was observed in BDL rats (SHAM: 0.6 vs. BDL: 0.32) (Fig. 6B,C).

Amyloid β The mean plasma levels of $A\beta_{42}$ were significantly decreased in BDL rats at week 8 compared to SHAM group (− 56%, $p < 0.05$). In addition, the $A\beta_{42}$/p-tau and $A\beta_{42}$/t-tau ratios were lower in BDL group compared to SHAM rats, 0.26 vs. 2.53 and 0.08 vs. 1.52, respectively (Fig. 6D).

MOG In case of neuronal damage, the myelin proteins are released into the bloodstream. The concentration of myelin oligodendrocyte glycoprotein in BDL rat plasma at week 8 was significantly higher (+ 295%, $p < 0.05$) than in the SHAM group (Fig. 6E).

GFAP Glial fibrillary acidic protein, a proxy of astrocyte reactivity, was quantified in plasma of BDL and SHAM rats. A significant increase of GFAP was observed in BDL rats at week 8 ($p < 0.001$) compared to the SHAM group where concentrations were below detection limit and attributed to the hypothetical value of 0 (Fig. 6F).

Plasma bile acids

BDL animals exhibited alterations in the bile acids profile (Fig. 7). A significant decrease of primary (including the murine forms) and secondary bile acids was seen. The pool of primary BAs decreased from 3198 to 32.5 ng/mL. The pool of murine forms of primary BAs decreased from 1154 to 139 ng/mL. The pool of secondary BAs decreased from 296.4 to 21.4 ng/mL. However, a significant increase of conjugated bile acids was observed. In particular, the taurine (tauro-α-muricholic acid (TαMCA), tauro-β-muricholic acid (TβMCA), tauroursodeoxycholic acid (TUDCA), taurochenodeoxycholic acid (TCDCA), and taurocholic acid (TCA)) conjugated bile acids caused

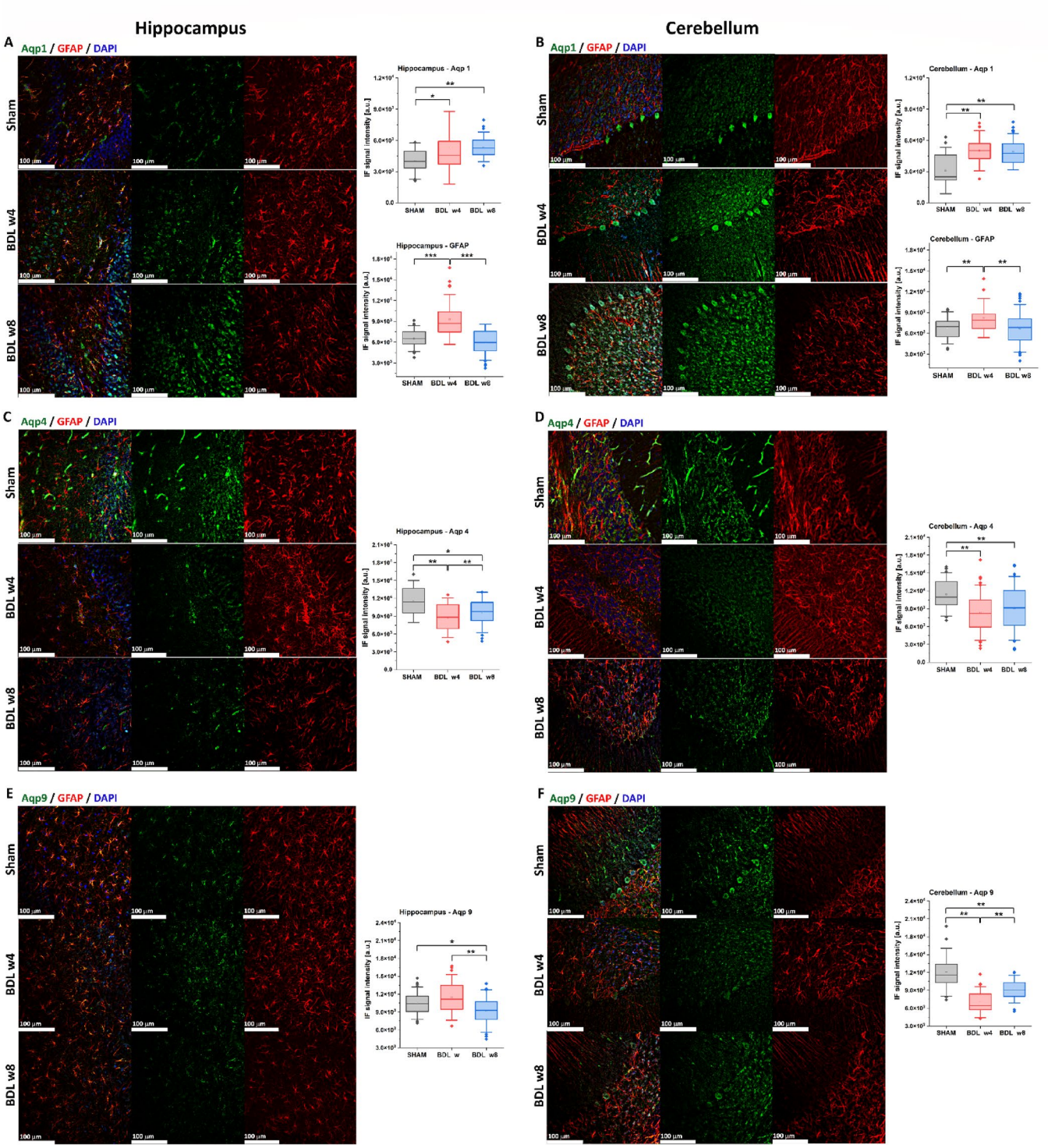

Fig. 5. **Representative micrographs showing immunostaining of Aqp1, Aqp4, Aqp9 and GFAP** in the hippocampus (left panel) and cerebellum (right panel) of BDL rats at week 4 and 8 post-surgery, and the control SHAM rats. Significant increase of immunolabeling with Aqp1 in BDL rats was visualized in the hippocampus (**A**) and cerebellum (**B**) and confirmed by the quantitative analyses in terms of the fluorescence intensity. Aqp4 expression visualized in vessels and astrocytic endfeet in SHAM rats in the hippocampus (**C**) and cerebellum (**D**) was significantly decreased in BDL rats, confirmed by the decrease of fluorescence intensity. Aqp9 expression decreased significantly in the hippocampal astrocytes (**E**) and the cerebellar Purkinje cells (soma and dendrites) and astrocytes (**F**), confirmed by the decrease of fluorescence intensity. GFAP—the quantitative analyses of the fluorescence intensity in the hippocampus (**A**) and cerebellum (**B**) showed an increase of the GFAP signal in BDL rats at week 4 and the overall decrease at week 8 corroborating with the immunolabeling. Data are presented as mean ± SD and statistical significance: $^{*}p < 0.05$, $^{**}p < 0.01$, $^{***}p < 0.001$(One-way Anova with post-hoc Tukey HSD). (For interpretation of the references to color in this figure legend, the reader is referred to the Web version of this article.)

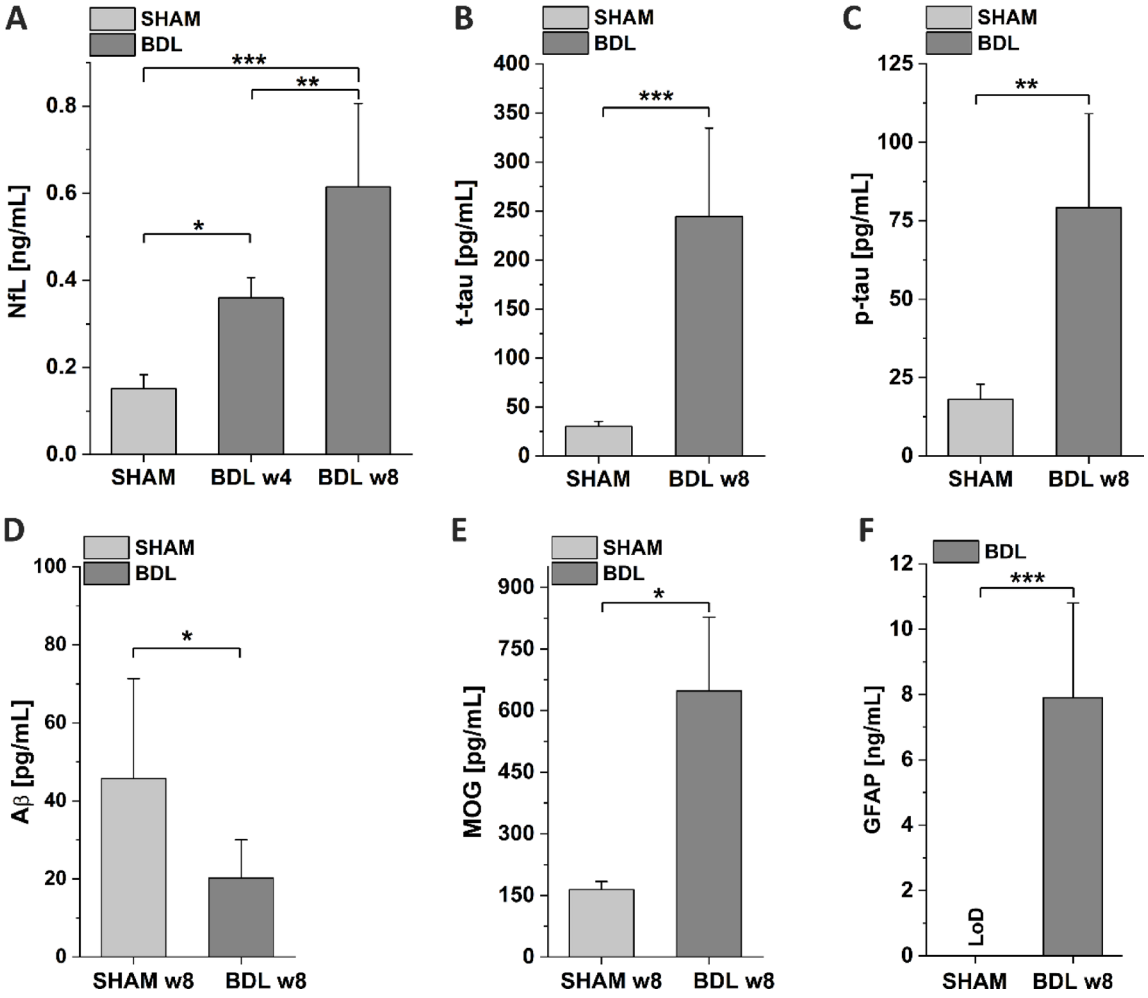

Fig. 6. Blood neurodegeneration markers quantification by ELISA assays. Comparison of plasma levels of (**A**) NfL, (**B**,**C**) tau-bodies, (**D**) Amyloid β_{42}, (**E**) MOG, and (**F**) GFAP between BDL and SHAM rats. Plasma NfL, tau-bodies, MOG, and GFAP levels were higher in the BDL group compared with SHAM controls, while amyloid β concentration decreased, all following the trends observed in Alzheimer Disease. Data are presented as mean ± SD and statistical significance: $^{*}p < 0.05$, $^{**}p < 0.01$, $^{***}p < 0.001$ (One-way Anova with post-hoc Tukey HSD).

an increase of total pool of BAs from 5424 to 76,514 ng/mL. In addition, an increased ratio of deoxycholic acid (DCA)/cholic acid (CA) (SHAM: 0.042 vs. BDL: 0.297, sevenfold change) was observed.

Discussion

This study demonstrates for the first time that chronic liver dysfunction can trigger Alzheimer's disease-related neuropathological hallmarks. By integrating histological, spectroscopic, and blood-based analyses, we show that BDL rats exhibit central and systemic markers of neurodegeneration compared with SHAM controls. These findings highlight the importance of assessing hepatic function in dementia diagnosis and support a systemic perspective on AD pathogenesis.

In AD, the intraneuronal accumulation of Aβ (iAβ) has been a subject of scientific debate since the 1980s and has been suggested to precede the formation of neurofibrillary tangles and the deposition of extracellular Aβ[22–24]. In the present study, for the first time in CLD rat model an intraneuronal accumulation of Aβ was observed in several brain regions together with tau-bodies in the pre-tangle and NFTs status, preceding extracellular plaque deposition, which aligns with early AD stages. Intraneuronal Aβ accumulation occurred concomitantly with neurofibrillary tangles formation in a time-dependent manner, increasing with disease progression.

Studies on transgenic mice (3xTg-AD mice) suggest that intraneuronal accumulation of Aβ plays a crucial role in triggering cognitive impairment, rather than its extracellular deposition, and correlates with deficits in synaptic transmission and long-term potentiation (LTP)[25,26]. Furthermore, the extracellular deposition occurs in the later stages of the disease and partly originates from iAβ in degenerating neurons[26]. Therefore, neurotoxicity initially attributed to extracellular Aβ may, in fact, represents a downstream consequence of earlier iAβ-mediated damage. Since adult BDL animals have a maximum lifespan of approximately 8 weeks post-surgery[16], it is likely

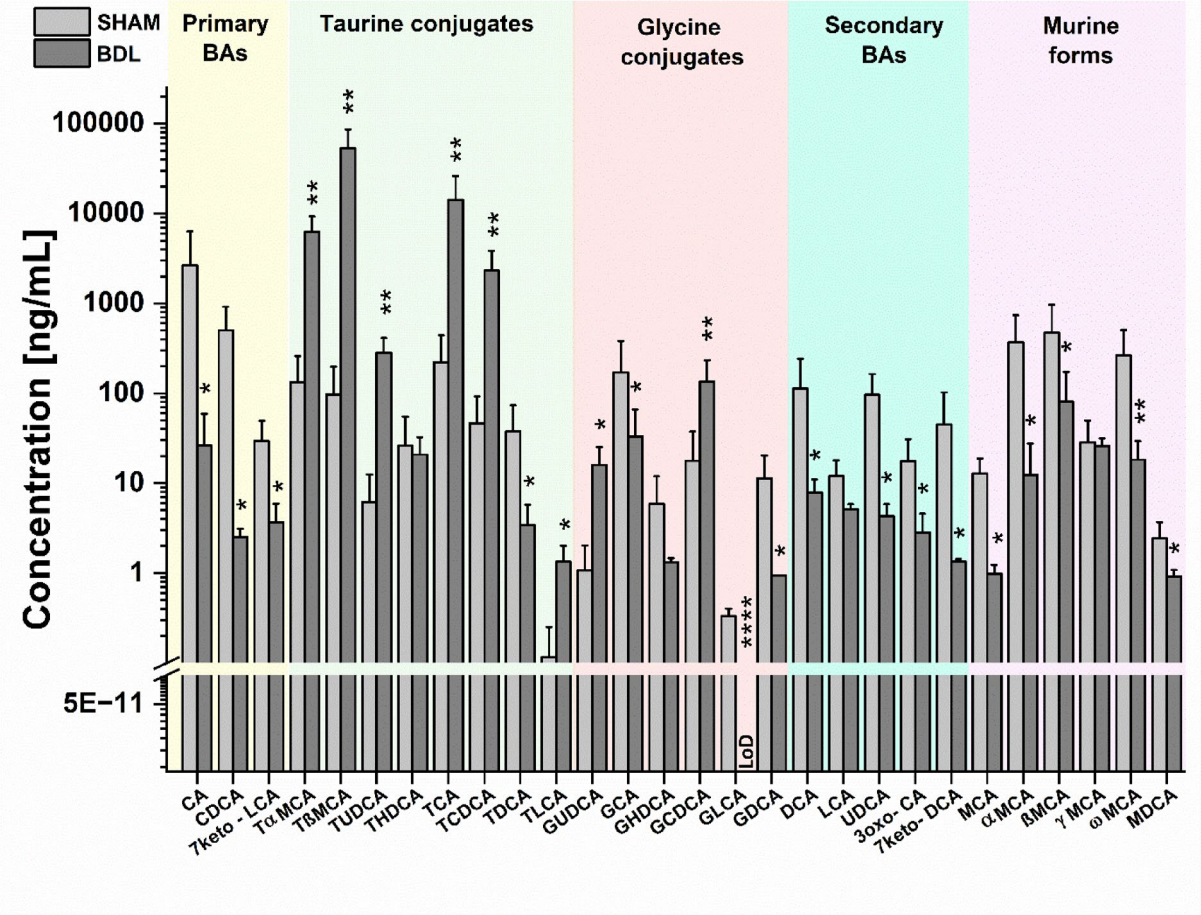

Fig. 7. **Comparison of plasma bile acids profiles of SHAM and BDL rats.** Data are presented as mean ± SD and statistical significance: $^{*}p < 0.05$, $^{**}p < 0.01$, $^{***}p < 0.001$, $^{****}p < 0.0001$ (One-way Anova with post-hoc Tukey HSD).

that the late-stage effects of extracellular Aβ accumulation, hallmarks of advanced AD, were not observed in our model.

The detected cerebral amyloid angiopathy (CAA) is likely due to impaired clearance of Aβ across the blood–brain barrier (BBB), suggesting a failure in the perivascular drainage of soluble Aβ from the brain[27]. This dysfunction weakens the blood vessels and increases the risk of intracerebral hemorrhage. It is thought to contribute to decreased cerebral blood flow, often present in type C HE[28], and is associated with an increased risk of cognitive impairment[29]. In addition, studies have revealed that Aβ causes vascular dysfunction via oxidative stress[30].

Oxidative stress is a major pathway driving neurodegeneration[10,12,31]. Neurons are highly sensitive to oxidative stress due to their high oxygen demand, relatively low antioxidant levels, the presence of high concentrations of unsaturated lipids, and metal ions[10]. The brain of both HE and AD patients as well as the brain of the CLD rat model, present significant extent of oxidative damage[10,12,31]. Moreover, in AD, oxidative damage has been associated with accumulation of Aβ and neurofibrillary tangles formation (aggregation and hyperphosphorylation of the tau protein)[32], something depicted also in the CLD rat model herein.

Aqp1, Aqp4, and Aqp9 are water channel proteins that maintain water balance and buffer extracellular ion concentrations. They have been identified in the mammalian brain and are produced under both healthy and pathological conditions[33–35]. Aquaporins also participate in various ancillary functions, such as glutamate clearance in tripartite synapses, neuronal excitation, neurotransmission, signal transduction, neurogenesis, and brain energy metabolism[35]. Additionally, they play a role in cell adhesion and migration[35].

Aqp 1 plays a pivotal role in maintaining water homeostasis[35,36], driven by the osmotic gradient[37] and thereby regulating cell volume[35]. Studies have shown increased Aqp1 expression in activated astrocytes in several neurodegenerative diseases, including AD, multiple sclerosis, epilepsy, and ischemia[33]. Quantitative analysis of Aqp1 immunofluorescence in the CLD rat model revealed a significant increase in signal as early as week 4 post-BDL in both studied brain regions, the hippocampus and cerebellum. Aqp1 immunofluorescence continued to increase in both, astrocytes processes and neurons, as the disease progressed. The observed increase in Aqp1 clearly indicates impaired water transport in the brain of the CLD rat model. Of note, studies in transgenic AD mice (3xTg-AD and 5xFAD) have shown a close association between Aqp1 upregulation and Aβ deposition,

highlighting the role of Aqp1 in Aβ clearance[33]. Furthermore, elevated Aqp1 expression can improve cell motility and Aβ clearance at amyloid deposition sites, indicating a response to Aβ-induced stress.

Aqp 4 is the primary water channel in the mammalian brain[37,38] contributing to neuronal excitability by maintaining osmotic balance and regulating the ionic environment around neurons[36]. Its decrease reported herein as early as week 4 post-BDL in both studied brain regions, the hippocampus and cerebellum, might play a protective role against brain swelling following the induction of cytotoxic edema[36] due to an increased ammonia load. Furthermore, the perivascular loss of Aqp4 has been reported in neurodegenerative and neurovascular disorders[39]. In AD, Aqp4 loss was specifically associated with Aβ plaque formation and tau pathology[37,40], as also depicted in this study.

Furthermore, studies in rodents with Aqp4 gene deletion revealed an increase in the apparent diffusion coefficient (ADC) of water, which was linked to altered brain fluid transport and an impaired glymphatic system[41–43]. This impairment slowed CSF influx and interstitial efflux, leading to interstitial fluid stagnation and enlargement of the interstitial space, thereby reducing Aβ clearance and resulting in increased Aβ deposition and further plaque formation[40,42,43]. Likewise, a modest elevation in the ADC of water has been observed in patients with type C HE[44]. This is most likely related to the outflow of solutes and waste products, the inflow of neurotoxins (such as ammonia), and the subsequent neuroinflammation and oxidative stress[10,12].

Aqp9 an aquaglyceroporin, plays a crucial role in brain energy homeostasis as a metabolite channel for energy substrates such as glycerol and monocarboxylates[42,45,46]. Quantitative analysis of Aqp9 immunofluorescence in the CLD rat model revealed a region-specific pattern of Aqp9 expression. A significant decrease in Aqp9 immunofluorescence was observed in the cerebellum as early as week 4 post-BDL, whereas a comparable reduction in the hippocampus emerged only by week 8. This temporal difference suggests that the cerebellum exhibits an earlier vulnerability to metabolic and osmotic stress compared to the hippocampus.

Given Aqp9 role in transporting glycerol and monocarboxylates, key substrates for energy metabolism[42,46], its early downregulation in the cerebellum may impair neuronal energy supply, potentially contributing to motor coordination deficits commonly associated with HE[47,48]. The later onset of Aqp9 decline in the hippocampus likely disrupts neuronal energy homeostasis at a more advanced stage, corroborating the progressive cognitive impairment/progressive memory deficits seen in CLD and AD[49].

Furthermore, the downregulation of Aqp9 may impair its role and significantly contribute to alterations in glucose metabolism, as demonstrated in our previous ^{18}F-FDG PET studies using the same CLD rat model[18], and aligns with findings of glucose hypometabolism in patient with decompensated cirrhosis[50].

Moreover, research using APP transgenic mice (APPswe/PS1dE9) indicated that Aqp9 downregulation could exacerbate Aβ-induced neurotoxicity, facilitate Aβ-mediated Alzheimer's disease progression, disrupt synaptic function, and promote apoptosis[46],thus, indicating the key role of Aqp9 in preserving neuronal vitality.

Glial fibrillary acidic protein is the main intermediary filament of astrocytes, the most abundant cell type in the CNS[51,52]. GFAP plays a central role in maintaining astrocyte morphology, myelination, and the integrity of the blood–brain barrier[53].

In the present study, GFAP immunolabeling followed by UV–Vis spectroscopy of immunofluorescence revealed a statistically significant increase in signal at week 4 post-BDL surgery, followed by a significant decrease at week 8 compared to week 4. These results corroborate our previous findings, which demonstrated cytoskeletal alterations in astrocytes in the CLD rat model, characterized by a decrease in processes and the number of intersections, along with changes in astrocyte numbers over disease progression[11,17,19]. This is a hallmark of astrocyte reactivity and a common feature of neuropathological disorders[54].

The loss of GFAP-positive cells and glial filaments may result from elevated brain ammonia, which is detoxified in astrocytes through glutamine synthesis, leading to osmotic and oxidative stress and accompanied by neuroinflammation (e.g., IL-6 accumulation in the CNS)[10–12,19]. Additionally, previously reported RNA oxidation can impair translation and gene expression, while oxidative stress may trigger protein depolymerization[10,12]. Because the cytoskeleton relies on an interconnected filament network stabilized by cross-linking proteins, damage to a single component can destabilize the entire structure, promoting OS-driven cytoskeletal breakdown and ultimately astrocytic cell death[10].

Furthermore, in healthy individuals, GFAP blood levels are generally very low and remain below the detection limits[53], as observed in SHAM group in this study. The significant increase in GFAP levels in the blood of BDL rats at week 8, as depicted here, aligns with a recent study on GFAP blood concentrations in cirrhotic patients[55]. This finding corroborates the previously observed astrocyte morphological alterations (injury) and activation in BDL rats[11,19], leading then to the observed increase of serum GFAP concentrations.

Alterations in GFAP expression and the loss of filaments (depolymerization) may play a major role in synaptic loss and changes in function[10,56]. These changes have been shown to closely correlate with reactive astrocytosis and elevated GFAP levels in both CSF and blood, and the density of neuritic plaques in the AD brain[56,57]. This further strengthens the argument for astrocytic activation as a mediator linking amyloid and tau pathology.

NfL is an axonal cytoskeleton component [20] that is mostly found in large myelinated axons. It is required for radial growth, structural integrity, and effective nerve impulse transmission[58]. Elevated NfL levels in bodily fluids (CSF and blood) have been linked to brain damage and atrophy[59] and correlated significantly with cognitive function impairment, particularly in those with neurological disorders[60,61]. Therefore, an increase of NfL levels in plasma of CLD rat model already at 4 weeks post BDL surgery is a clear sign of neuroaxonal damage. Furthermore, recent studies have reported a significant relationship between blood NfL levels and brain atrophy in AD pathology, with elevated concentrations detectable even in the preclinical stages of the disease[59].

Tau's principal physiological role is to maintain microtubules within neuronal axons[62]. The neurodegenerative processes leads to neurofibrillary tangles formation and increased release of tau into the CSF and bloodstream[63], something observed here in the rat model of CLD. Studies have shown a significant relationship between plasma p-tau concentration, cognitive decline, brain atrophy, and glucose hypometabolism[64,65]. Eelevated p-tau levels

in patients with subjective cognitive decline (SCD) and mild cognitive impairment (MCI) strongly predicted their progression to AD[66]. Furthermore, a reduced p/t-tau ratio, as observed in this study, has been shown to be a strong predictor of future AD[67].

Amyloid β is the main component of the amyloid plaques found in AD brains[68]. Studies have shown reduced $A\beta_{42}$ levels in the plasma of AD patients[68]. Similarly, a decrease in $A\beta_{42}$ levels was observed in this study in CLD rat model. It has also been reported that the $A\beta_{42}$/p-tau and $A\beta_{42}$/t-tau ratios significantly decrease in the CSF of AD patients[69]. Consistently, decreased $A\beta_{42}$/p-tau and $A\beta_{42}$/t-tau ratios were observed in the CLD rat model in this study.

Myelin degeneration is believed to contribute to neuronal dysfunction and is associated with Aβ plaque accumulation and tau hyperphosphorylation, ultimately leading to cognitive decline[70]. Myelin oligodendrocyte glycoprotein is an immunoglobulin (autoantigen)[71] expressed exclusively in CNS, located in the outermost layer of the myelin membrane[72] being a marker of oligodendrocytes maturity and possibly playing a role in cell adhesion and microtubule stability[71]. The elevated MOG levels observed in BDL rats may indicate oligodendrocyte membrane damage, resulting in a higher efflux of MOG into the bloodstream.

Bile acids play a crucial role in CNS physiology, and alterations in bile acid profiles have been associated with neurodegenerative disorders[73]. Under physiological conditions, the bile acids pool is carefully controlled[74]. An increase in the total bile acid pool concentration is directly linked to liver damage[74]. A reduction in primary bile acids, as observed here, have been linked to gut microbiota imbalance, impaired lipid digestion, and disrupted enterohepatic circulation[10,73]. A 100-fold decrease of primary and tenfold decrease of secondary bile acids in BDL rats resulted in an elevated deoxycholic acid (DCA) to cholic acid (CA) ratio, indicative of the 7α-dehydroxylation of CA by gut bacteria. Studies have shown that an increased DCA/CA ratio is associated with cognitive decline, indicating a potential role of gut-liver-brain axis in the pathogenesis of neurodegenerative diseases[4]. Recent studies support that gut microbiota influences pathological features of Alzheimer's disease, including neuroinflammation and Aβ accumulation[73].

In addition, the enteric nervous system connects the gut microbiota with the CNS via vagal signaling, forming a key pathway of the gut-liver-brain axis[10]. As a result, bacterial infections / microbiota alterations and systemic inflammatory responses can alter brain function by stimulating afferent vagal pathways, a process driven by the release of cytokines and chemokines at sites of inflammation, which may subsequently impair cognitive and motor performance[10,75].

Furthermore, the increased concentration of taurochenodeoxycholic acid (TCDCA), as reported here, has been associated with a decreased mitochondrial membrane potential[73], a hallmark of mitochondrial disfunction that may lead to loss of cell viability and contribute to various pathologies[76]. In particular, association between bile acids and oxidative stress have been well demonstrated[77]. The release of ROS may result in depletion of antioxidants, oxidation of thiol groups and lipid peroxidation[10,77].

Conclusions

This is the first study to our knowledge to demonstrate a direct association between liver function and the risk of Alzheimer's disease. Our results provide further evidence of liver implication in Aβ and tau accumulation. Although these associations are robust, the underlying mechanisms still need to be clarified.

Our findings offer valuable insights for future research into the link between liver function and AD pathogenesis, as well as for developing prevention and treatment strategies that address liver dysfunction. In particular, our work introduces a novel preclinical paradigm that bridges hepatology and neurology, shifting the conventional brain-centric view of AD toward a systemic disease model.

Importantly, these results highlight the need for a more holistic and physiological approach to AD and other dementias, considering patient comorbidities and adopting a multidisciplinary strategy to study the pathobiology of AD and other dementias.

Materials and methods'

Animal welfare

In line with the 3R (Replacement, Reduction, and Refinement) principles, the rats used in the current study have been previously described and characterized in earlier publications [11,19]. In the current study a range of additional histological stainings and blood analyses were conducted. As such, no additional animals were euthanized for this work. All procedures were done in accordance with the animal care and were approved by The Committee on Animal Experimentation for the Canton de Vaud, Switzerland (VD3022) and complied with the ARRIVE guidelines.

Chronic liver disease model

Wistar male adult rats (BDL n = 31, SHAM n = 18, Charles River Laboratories, L'Arbresle, France) were group-housed in the animal facilities of CIBM-AIT in Lausanne for BDL experiments. The BDL model was selected to represent chronic liver disease (CLD) because it reliably induces cholestatic liver injury and fibrosis within a predictable timeframe[16]. Animals underwent bile-duct ligation (BDL—recordings of surgery steps: https://zenodo.org/records/10652104) for CLD-induced HE, recognized by the International Society for Hepatic Encephalopathy and Nitrogen Metabolism (ISHEN[16]), and sham surgery. The Supplementary Material & Methods contains a detailed information about the number of animals used for each experiment (Table S1).

Biochemical measurements

Chronic liver disease was confirmed by the early increase in plasma ammonia and bilirubin at 2 weeks post-BDL. Liver parameters were monitored longitudinally at weeks 0, 2, 4, 6, and 8. Plasma bilirubin, aspartate

aminotransferase (AST/GOT), and alanine aminotransferase (ALT/GPT) were measured using the Reflotron® Plus system (F. Hoffmann-La Roche Ltd), blood ammonia was assessed with a blood ammonia meter (PocketChem™ BA PA-4140), and blood glucose levels were determined using the Contour XT (Bayer, Germany), as previously reported[12].

Blood samples (BDL n = 31, SHAM n = 18) were taken from the sublingual vein into anti-coagulated tubes (EDTA). Blood was collected in pre-cooled K3EDTA tubes (Sarstedt AG & Co. KG), centrifuged at 2,700 × g for 7 min at 4 °C, and stored at − 80 °C until the assay procedure.

Histology

Rats were pre-anesthetized with 4% isoflurane (Piramal Enterprises Ltd.) for 5 min, followed by a subcutaneous injection of the analgesic Temgesic (ESSEX) at 0.03 mg/mL in 0.9% NaCl. Fifteen minutes later, an intracardiac perfusion was performed via the left ventricle using phosphate-buffered saline (PBS, P5493 Sigma, pH 7.4). Following perfusion, the animals were euthanized by decapitation. The brains were then removed, fixed in 4% formaldehyde in PBS overnight at 4 °C, washed with PBS, and embedded in paraffin. The brains were sectioned into 8 µm thick sagittal sections for standard histochemistry (4-weeks (n = 3) and 8-weeks (n = 3) post-BDL and SHAM (n = 3) surgery). For immunohistochemistry after 4% formaldehyde fixation brains were cryopreserved in 30% sucrose PBS solution at 4 °C for 48 h, and then embedded in Tissue-Tek O.C.T. compound and then cut into 16 µm sagittal-sections (4-weeks (n = 3) and 8-weeks (n = 3) post-BDL and SHAM (n = 3) surgery). For both techniques a 7 slides/rat were used (histochemistry: 126 slides prepared, immunohistochemistry: 189 slides prepared).

The selected 4- and 8-week (humane endpoint) intervals allow for longitudinal assessment of histological changes during the progression of chronic liver disease.

Histochemistry

Amyloid β pathology

Congo Red staining (CR protocol, IHC WORLD, LLC) was used to determine Amyloid pathology https://ihcworld.com/2024/01/26/modified-high-ph-congo-red-staining-protocol-for-amyloid/.

Tau protein pathology

The Gallyas Silver Stain technique was used to investigate tau protein pathology according to the protocol described in GS protocol https://www.protocolsonline.com/histology/dyes-and-stains/neurohistology/gallyas-silver-stain/ .

For both staining's slides were deparaffinized and rehydrated in distilled water before being incubated in working solution and washed in distilled water. Finally, they were differentiated and then dehydrated through a graded series of ethanol's, washed in xylene, and mounted in resinous mounting media.

Tissue sections were examined using bright field microscopy with a MEIJI-TECHNO TC5600 microscope. Images were captured and processed using INFINITY ANALYZE 7 software (Lumenera, Canada).

Immunohistochemistry and immunofluorescence (UV–Vis spectroscopy)

Two brain regions were selected for immunohistochemical analysis: the hippocampus and the cerebellum. The hippocampus was examined as it is one of the earliest structures affected in Alzheimer's disease and is critically involved in cognitive and non-cognitive functions. The cerebellum was included due to its essential role in the regulation and maintenance of these processes[78,79]. Three sets of tissue sections were incubated with a polyclonal rabbit anti-aquaporin antibody: Aqp1 (PA5-77842, Thermo Fisher) (2 h at RT) at 1/100 dilution, Aqp4 C-terminus (PA5-77716, Thermo Fisher) (2 h at RT) at 1/200 dilution, Aqp9 (PA5-114872, Thermo Fisher) (2 h at RT) at 1/100 dilution with Alexa Fluor® Plus 488 secondary goat anti rabbit antibody IgG (H + L, A32731, Thermo Fisher) (1 h at RT) at 1/1000 dilution and then counterstained with mouse monoclonal anti-GFAP antibody (glia-specific intermediate-filament protein, MAB360, Merck Millipore)(2 h at RT) at 1/100 dilution with secondary Alexa Fluor® 594-AffiniPure rat anti-mouse IgG (H + L) antibody (415-585-166, Jackson ImmunoResearch Europe Ltd.) (1 h at RT) at 1/200 dilution were used to visualize astrocytes. Nuclei were stained with DAPI (D1306, Thermo Fisher).

The Leica THUNDER Imaging System was integrated with the Ocean HDX UV–Vis spectrometer (Ocean Insight, Florida, USA) and the Lab Grade Reflection Probe R400-7-UV–VIS. Fluorophore signals were captured using excitation, dichroic, and emission filter sets (Chroma Technology Corporation: EM: ET610lp, BS: ZT594rdc, EX: ET580/25) to detect fluorescence signals. The total Aqp1, Aqp4, Aqp9, and GFAP signal intensities were quantified by integrating the UV–Vis spectra. Spectra were evaluated and processed by OriginPro (OriginLab, USA).

Determination of blood neurodegeneration markers

Neurofilament quantification

Quantitative determination of neurofilament light chain (NfL) levels was performed in plasma samples from BDL (4-weeks n = 6 and 8-weeks n = 10) and SHAM (n = 4) rats. Plasma NfL levels were measured in duplicate using ELISA NfL kit, according to the manufacturer's instructions and standard procedures (CUSABIO: CSB-EL015688RA, analytical sensitivity: 1.95 pg/mL, detection range: 7.8–500 pg/mL).

Phosphorylated p-tau and total t-tau quantification

The levels of p-tau and t-tau were determined in plasma samples from BDL (8-weeks n = 4) and SHAM (n = 3) rats. Plasma p-tau and t-tau levels were measured in duplicate using ELISA p-tau (AssayGenie: RTFI01098, analytical sensitivity: 9.375 pg/mL, detection range: 15.625–1000 pg/mL) and t- tau kits (AssayGenie: RTFI00944,

analytical sensitivity: 18.75 pg/mL, detection range: 31.25–2000 pg/mL), according to the manufacturer's instructions and standard procedures.

Amyloid β quantification
Quantitative determination of amyloid β (Aβ) levels, was performed in plasma samples from BDL (8-weeks n = 5) and SHAM (n = 6) rats. Plasma Aβ levels were measured in duplicate using ELISA Aβ kit (Invitrogen: KMB3441, analytical sensitivity: < 3 pg/mL, detection range: 3.12–200 pg/mL), according to the manufacturer's instructions and standard procedures.

GFAP quantification
GFAP levels were determined in plasma samples from BDL (8-weeks n = 8) and SHAM (n = 6) rats using the highly sensitive Rat GFAP ELISA Kit (AssayGenie: RTES00998, sensitvity: 0.19 ng/mL, detection range: 0.31–20 ng/mL). Samples were measured in duplicate according to the manufacturer's instructions.

Myelin oligodendrocyte glycoprotein (MOG) quantification
The levels of MOG were determined in plasma samples from adult (8-weeks n = 9) and SHAM (n = 4) rats. Plasma MOG levels were measured in duplicate using ELISA MOG (AVIVA SYSTEMS BIOLOGY: OKCD00239, analytical sensitivity: 0.055 ng/mL, detection range: 0.156–10 ng/mL) kit, according to the manufacturer's instructions and standard procedures.

The absorbance was measured at 450 nm with microplate reader Hidex Sense Beta (Hidex Oy).

Plasma bile acids

Isotope-dilution high performance liquid chromatography coupled to high resolution mass spectrometry (LC–MS) was used[80] to measure the bile acids at 8 weeks after BDL (n = 7) and SHAM (n = 8) surgery. The experiment was carried out by mixing the specimen (50 µL) with the internal standards in methanol (100 µL) and then adding 600 µL of H_2O containing 0.2% formic acid. HLB SPE plates (Waters) were used for sample extraction and cleaning. Thermo Q-Exactive (Thermo Fisher Scientific) was used for LC–MS analysis. A 10 µL extract volume was injected into an Acquity UPLC HSS T3 1.8 µm, 2.1 100 mm column. The MS was set to full-scan acquisition in negative mode (-H m/z 370 to 522, centroid acquisition, negative polarity).

Statistical analysis

For ELISA and UV–Vis spectroscopy one-way ANOVA followed by post-hoc Turkey HSD was used to compare BDL and SHAM-operated rats, except for the GFAP and GLCA bile acid level in the blood, which were analyzed using a one-sample Student's t-test against a hypothetical value of 0, as the levels in SHAM (GFAP) and BDL (GLCA bile acid) rats were below the detection limit. All tests were 2-tailed, Significance level in all tests was attributed as follows: $^{*}p < 0.05$, $^{**}p < 0.01$, $^{***}p < 0.001$, $^{****}p < 0.0001$. Statistical analyses were performed using OriginPro (OriginLab, USA).

Study limitations
One of the limitations of this study is the exclusive use of male rats, which may limit the generalizability of the findings to both sexes, as sex differences in liver disease progression and AD vulnerability may affect outcomes. More work with both male and female rats is necessary to determine whether these results are consistent across sexes. Additionally, the absence of behavioral assessments is a limitation of the present study, as such measures could provide important insights into functional consequences of the observed changes. To address these issues, we have now initiated experiments using female rats to explore potential sex-specific differences.

Data availability

The data used to support the findings of this study are available from the corresponding author upon request.

Received: 3 June 2025; Accepted: 18 September 2025
Published online: 30 October 2025

References

1. Prince, M. J. et al. World Alzheimer report 2015—The global impact of dementia: An analysis of prevalence, incidence, cost and trends. *Alzheimer's Dis. Internatl. (ADI)* (2015).
2. Alzheimer's, A. 2024 Alzheimer's disease facts and figures. *Alzheimers Dement* **20**, 3708–3821. https://doi.org/10.1002/alz.13809 (2024).
3. Barthelemy, N. R. et al. A soluble phosphorylated tau signature links tau, amyloid and the evolution of stages of dominantly inherited Alzheimer's disease. *Nat. Med.* **26**, 398–407. https://doi.org/10.1038/s41591-020-0781-z (2020).
4. Bassendine, M. F., Taylor-Robinson, S. D., Fertleman, M., Khan, M. & Neely, D. Is Alzheimer's Disease a liver disease of the brain?. *J. Alzheimers Dis.* **75**, 1–14. https://doi.org/10.3233/JAD-190848 (2020).
5. Zolezzi, J. M., Bastias-Candia, S., Santos, M. J. & Inestrosa, N. C. Alzheimer's disease: Relevant molecular and physiopathological events affecting amyloid-beta brain balance and the putative role of PPARs. *Front. Aging Neurosci.* **6**, 176. https://doi.org/10.3389/fnagi.2014.00176 (2014).
6. Li, X., Wen, D. X., Zhao, Y. H., Hang, Y. N. & Mandell, M. S. Increase of beta-amyloid and C-reactive protein in liver transplant recipients with postoperative cognitive dysfunction. *Hepatobiliary Pancreat. Dis. Int.* **12**, 370–376. https://doi.org/10.1016/s1499-3872(13)60058-2 (2013).
7. Chen, T. B. et al. Comorbidity and dementia: A nationwide survey in Taiwan. *PLoS ONE* **12**, e0175475. https://doi.org/10.1371/journal.pone.0175475 (2017).
8. Bajaj, J. S. et al. Undiagnosed cirrhosis and hepatic encephalopathy in a national cohort of veterans with dementia. *JAMA Netw. Open* **7**, e2353965. https://doi.org/10.1001/jamanetworkopen.2023.53965 (2024).

9. Estrada, L. D., Ahumada, P., Cabrera, D. & Arab, J. P. Liver dysfunction as a novel player in Alzheimer's progression: Looking outside the brain. *Front. Aging Neurosci.* **11**, 174. https://doi.org/10.3389/fnagi.2019.00174 (2019).
10. Simicic, D., Cudalbu, C. & Pierzchala, K. Overview of oxidative stress findings in hepatic encephalopathy: From cellular and ammonium-based animal models to human data. *Anal. Biochem.* **654**, 114795. https://doi.org/10.1016/j.ab.2022.114795 (2022).
11. Braissant, O. et al. Longitudinal neurometabolic changes in the hippocampus of a rat model of chronic hepatic encephalopathy. *J. Hepatol.* **71**, 505–515. https://doi.org/10.1016/j.jhep.2019.05.022 (2019).
12. Pierzchala, K. et al. Central nervous system and systemic oxidative stress interplay with inflammation in a bile duct ligation rat model of type C hepatic encephalopathy. *Free Radic. Biol. Med.* **178**, 295–307. https://doi.org/10.1016/j.freeradbiomed.2021.12.011 (2022).
13. Garcia-Garcia, R. et al. Learning and memory impairments in patients with minimal hepatic encephalopathy are associated with structural and functional connectivity alterations in hippocampus. *Sci. Rep.* **8**, 9664. https://doi.org/10.1038/s41598-018-27978-x (2018).
14. Fisman, M. et al. Hyperammonemia in Alzheimer's disease. *Am. J. Psychiatry* **142**, 71–73. https://doi.org/10.1176/ajp.142.1.71 (1985).
15. Nho, K. et al. Association of altered liver enzymes with Alzheimer disease diagnosis, cognition, neuroimaging measures, and cerebrospinal fluid biomarkers. *JAMA Netw. Open* **2**, e197978. https://doi.org/10.1001/jamanetworkopen.2019.7978 (2019).
16. DeMorrow, S., Cudalbu, C., Davies, N., Jayakumar, A. R. & Rose, C. F. 2021 ISHEN guidelines on animal models of hepatic encephalopathy. *Liver Int.* **41**, 1474–1488. https://doi.org/10.1111/liv.14911 (2021).
17. Mosso, J. et al. Diffusion of brain metabolites highlights altered brain microstructure in type C hepatic encephalopathy: a 9.4 T preliminary study. *Front. Neurosci.* **18**, 1344076, https://doi.org/10.3389/fnins.2024.1344076 (2024).
18. Mosso, J. et al. PET CMR(glc) mapping and (1)H-MRS show altered glucose uptake and neurometabolic profiles in BDL rats. *Anal. Biochem.* **647**, 114606. https://doi.org/10.1016/j.ab.2022.114606 (2022).
19. Simicic, D. et al. Differential metabolic and cellular brain regional susceptibility in adult rats with chronic liver disease. arXiv:2503.20073 (2025).
20. Srpova, B. et al. Serum neurofilament light chain reflects inflammation-driven neurodegeneration and predicts delayed brain volume loss in early stage of multiple sclerosis. *Mult. Scler.* **27**, 52–60. https://doi.org/10.1177/1352458519901272 (2021).
21. Gordillo-Escobar, E., Egea-Guerrero, J. J., Rodriguez-Rodriguez, A. & Murillo-Cabezas, F. Usefulness of biomarkers in the prognosis of severe head injuries. *Med. Intensiva.* **40**, 105–112. https://doi.org/10.1016/j.medin.2015.11.008 (2016).
22. Grundke-Iqbal, I. et al. Amyloid protein and neurofibrillary tangles coexist in the same neuron in Alzheimer disease. *Proc. Natl. Acad. Sci. U S A* **86**, 2853–2857. https://doi.org/10.1073/pnas.86.8.2853 (1989).
23. Gouras, G. K. et al. Intraneuronal Abeta42 accumulation in human brain. *Am. J. Pathol.* **156**, 15–20. https://doi.org/10.1016/s0002-9440(10)64700-1 (2000).
24. Masters, C. L. et al. Neuronal origin of a cerebral amyloid: Neurofibrillary tangles of Alzheimer's disease contain the same protein as the amyloid of plaque cores and blood vessels. *EMBO J.* **4**(11), 2757–2763. https://doi.org/10.1002/j.1460-2075.1985.tb04000.x (1985).
25. Billings, L. M., Oddo, S., Green, K. N., McGaugh, J. L. & LaFerla, F. M. Intraneuronal Abeta causes the onset of early Alzheimer's disease-related cognitive deficits in transgenic mice. *Neuron* **45**, 675–688. https://doi.org/10.1016/j.neuron.2005.01.040 (2005).
26. Moon, M. et al. Intracellular Amyloid-β accumulation in calcium-binding protein-deficient neurons leads to Amyloid-β plaque formation in animal model of Alzheimer's disease. *J. Alzheimers Dis.* **29**, 615–628. https://doi.org/10.3233/Jad-2011-111778 (2012).
27. Hawkes, C. A., Jayakody, N., Johnston, D. A., Bechmann, I. & Carare, R. O. Failure of perivascular drainage of beta-amyloid in cerebral amyloid angiopathy. *Brain Pathol.* **24**, 396–403. https://doi.org/10.1111/bpa.12159 (2014).
28. Dam, G. et al. Hepatic encephalopathy is associated with decreased cerebral oxygen metabolism and blood flow, not increased ammonia uptake. *Hepatology* **57**, 258–265. https://doi.org/10.1002/hep.25995 (2013).
29. Jakel, L., De Kort, A. M., Klijn, C. J. M., Schreuder, F. & Verbeek, M. M. Prevalence of cerebral amyloid angiopathy: A systematic review and meta-analysis. *Alzheimers Dement* **18**, 10–28. https://doi.org/10.1002/alz.12366 (2022).
30. Park, L. et al. Brain perivascular macrophages initiate the neurovascular dysfunction of Alzheimer abeta peptides. *Circ. Res.* **121**, 258–269. https://doi.org/10.1161/CIRCRESAHA.117.311054 (2017).
31. Huang, W. J., Zhang, X. & Chen, W. W. Role of oxidative stress in Alzheimer's disease. *Biomed Rep.* **4**, 519–522. https://doi.org/10.3892/br.2016.630 (2016).
32. Christen, Y. Oxidative stress and Alzheimer disease. *Am. J. Clin. Nutr.* **71**, 621S-629S. https://doi.org/10.1093/ajcn/71.2.621s (2000).
33. Park, J. et al. Neuronal Aquaporin 1 inhibits amyloidogenesis by suppressing the interaction between beta-secretase and amyloid precursor protein. *J. Gerontol .A Biol. Sci. Med. Sci.* **76**, 23–31. https://doi.org/10.1093/gerona/glaa068 (2021).
34. Amro, Z., Ryan, M., Collins-Praino, L. E. & Yool, A. J. Unexpected classes of aquaporin channels detected by transcriptomic analysis in human brain are associated with both patient age and Alzheimer's disease status. *Biomedicines* **11**, https://doi.org/10.3390/biomedicines11030770 (2023).
35. Zhou, Z. et al. The water transport system in Astrocytes-Aquaporins. *Cells* **11**, https://doi.org/10.3390/cells11162564 (2022).
36. Satoh, J., Tabunoki, H., Yamamura, T., Arima, K. & Konno, H. Human astrocytes express aquaporin-1 and aquaporin-4 in vitro and in vivo. *Neuropathology* **27**, 245–256. https://doi.org/10.1111/j.1440-1789.2007.00774.x (2007).
37. Potokar, M., Jorgacevski, J. & Zorec, R. Astrocyte Aquaporin Dynamics in Health and Disease. *Int J. Mol. Sci.* **17**, https://doi.org/10.3390/ijms17071121 (2016).
38. Gunnarson, E., Zelenina, M. & Aperia, A. Regulation of brain aquaporins. *Neuroscience* **129**, 947–955. https://doi.org/10.1016/j.neuroscience.2004.08.022 (2004).
39. Badaut, J. et al. Distribution of Aquaporin 9 in the adult rat brain: preferential expression in catecholaminergic neurons and in glial cells. *Neuroscience* **128**, 27–38. https://doi.org/10.1016/j.neuroscience.2004.05.042 (2004).
40. Xu, Z. et al. Deletion of aquaporin-4 in APP/PS1 mice exacerbates brain Abeta accumulation and memory deficits. *Mol. Neurodegener* **10**, 58. https://doi.org/10.1186/s13024-015-0056-1 (2015).
41. Salman, M. M. et al. Emerging roles for dynamic aquaporin-4 subcellular relocalization in CNS water homeostasis. *Brain* **145**, 64–75. https://doi.org/10.1093/brain/awab311 (2022).
42. Hirt, L., Price, M., Benakis, C. & Badaut, J. Aquaporins in neurological disorders. *Clin. Trans. Neurosci.* https://doi.org/10.1177/2514183x17752902 (2018).
43. Gomolka, R. S. et al. Loss of aquaporin-4 results in glymphatic system dysfunction via brain-wide interstitial fluid stagnation. *Elife* **12**, https://doi.org/10.7554/eLife.82232 (2023).
44. Kale, R. A. et al. Demonstration of interstitial cerebral edema with diffusion tensor MR imaging in type C hepatic encephalopathy. *Hepatology* **43**, 698–706. https://doi.org/10.1002/hep.21114 (2006).
45. Arcienega, II, Brunet, J. F., Bloch, J. & Badaut, J. Cell locations for AQP1, AQP4 and 9 in the non-human primate brain. *Neuroscience* **167**, 1103–1114, https://doi.org/10.1016/j.neuroscience.2010.02.059 (2010).
46. Liu, J. Y. et al. Downregulation of aquaporin 9 exacerbates beta-amyloid-induced neurotoxicity in Alzheimer's disease models in vitro and in vivo. *Neuroscience* **394**, 72–82. https://doi.org/10.1016/j.neuroscience.2018.09.016 (2018).
47. Urios, A. et al. Altered postural control and stability in cirrhotic patients with minimal hepatic encephalopathy correlate with cognitive deficits. *Liver Int.* **37**, 1013–1022. https://doi.org/10.1111/liv.13345 (2017).

48. San Martin-Valenzuela, C. et al. Motor and cognitive performance in patients with liver cirrhosis with minimal hepatic encephalopathy. *J. Clin. Med.* https://doi.org/10.3390/jcm9072154 (2020).
49. Song, D., Li, Y., Yang, L. L., Luo, Y. X. & Yao, X. Q. Bridging systemic metabolic dysfunction and Alzheimer's disease: the liver interface. *Mol. Neurodegener.* **20**, 61. https://doi.org/10.1186/s13024-025-00849-6 (2025).
50. Vankadari, K. et al. Detection of hepatic encephalopathy on 18F-FDG PET/CT brain images in a patient with decompensated liver cirrhosis. *Clin. Nucl. Med.* **43**, e486–e487. https://doi.org/10.1097/RLU.0000000000002327 (2018).
51. Sullivan, S. M. GFAP variants in health and disease: Stars of the brain and gut. *J. Neurochem.* **130**, 729–732. https://doi.org/10.1111/jnc.12754 (2014).
52. Eng, L. F., Ghirnikar, R. S. & Lee, Y. L. Glial fibrillary acidic protein: GFAP-thirty-one years (1969–2000). *Neurochem. Res.* **25**, 1439–1451. https://doi.org/10.1023/a:1007677003387 (2000).
53. Mayer, C. A. et al. Blood levels of glial fibrillary acidic protein (GFAP) in patients with neurological diseases. *PLoS ONE* **8**, e62101. https://doi.org/10.1371/journal.pone.0062101 (2013).
54. Zhou, B., Zuo, Y. X. & Jiang, R. T. Astrocyte morphology: Diversity, plasticity, and role in neurological diseases. *CNS Neurosci. Ther.* **25**, 665–673. https://doi.org/10.1111/cns.13123 (2019).
55. Gairing, S. J. et al. Elevated serum levels of glial fibrillary acidic protein are associated with covert hepatic encephalopathy in patients with cirrhosis. *JHEP Rep.* **5**, 100671. https://doi.org/10.1016/j.jhepr.2023.100671 (2023).
56. Middeldorp, J. & Hol, E. M. GFAP in health and disease. *Prog. Neurobiol.* **93**, 421–443. https://doi.org/10.1016/j.pneurobio.2011.01.005 (2011).
57. Sanchez-Juan, P. et al. Serum GFAP levels correlate with astrocyte reactivity, post-mortem brain atrophy and neurofibrillary tangles. *Brain* **147**, 1667–1679. https://doi.org/10.1093/brain/awae035 (2024).
58. Andersson, E. et al. Blood and cerebrospinal fluid neurofilament light differentially detect neurodegeneration in early Alzheimer's disease. *Neurobiol. Aging* **95**, 143–153. https://doi.org/10.1016/j.neurobiolaging.2020.07.018 (2020).
59. Jung, Y. & Damoiseaux, J. S. The potential of blood neurofilament light as a marker of neurodegeneration for Alzheimer's disease. *Brain* **147**, 12–25. https://doi.org/10.1093/brain/awad267 (2024).
60. Khalil, M. et al. Neurofilaments as biomarkers in neurological disorders. *Nat. Rev. Neurol.* **14**, 577–589. https://doi.org/10.1038/s41582-018-0058-z (2018).
61. Gaiottino, J. et al. Increased neurofilament light chain blood levels in neurodegenerative neurological diseases. *PLoS ONE* **8**, e75091. https://doi.org/10.1371/journal.pone.0075091 (2013).
62. Avila, J., Lucas, J. J., Pérez, M. & Hernández, F. Role of tau protein in both physiological and pathological conditions. *Physiol. Rev.* **84**, 361–384. https://doi.org/10.1152/physrev.00024.2003 (2004).
63. Zetterberg, H. Review: Tau in biofluids—relation to pathology, imaging and clinical features. *Neuropath. Appl. Neuro.* **43**, 194–199. https://doi.org/10.1111/nan.12378 (2017).
64. Mattsson, N. et al. Plasma tau in Alzheimer disease. *Neurology* **87**, 1827–1835. https://doi.org/10.1212/Wnl.0000000000003246 (2016).
65. Landau, S. M. et al. Amyloid deposition, hypometabolism, and longitudinal cognitive decline. *Ann. Neurol.* **72**, 578–586. https://doi.org/10.1002/ana.23650 (2012).
66. Palmqvist, S. et al. Prediction of future Alzheimer's disease dementia using plasma phospho-tau combined with other accessible measures. *Nat. Med.* **27**, 1034–1042. https://doi.org/10.1038/s41591-021-01348-z (2021).
67. Tondelli, M. et al. Predictive value of phospho-tau/total-tau ratio in amyloid-negative mild cognitive impairment. *Neurosci. Lett.* **787**, 136811. https://doi.org/10.1016/j.neulet.2022.136811 (2022).
68. Klyucherev, T. O. et al. Advances in the development of new biomarkers for Alzheimer's disease. *Transl. Neurodegener* **11**, 25. https://doi.org/10.1186/s40035-022-00296-z (2022).
69. de Jong, D., Jansen, R. W., Kremer, B. P. & Verbeek, M. M. Cerebrospinal fluid amyloid beta42/phosphorylated tau ratio discriminates between Alzheimer's disease and vascular dementia. *J. Gerontol. A Biol. Sci. Med. Sci.* **61**, 755–758. https://doi.org/10.1093/gerona/61.7.755 (2006).
70. Papuc, E. & Rejdak, K. The role of myelin damage in Alzheimer's disease pathology. *Arch. Med. Sci.* **16**, 345–351. https://doi.org/10.5114/aoms.2018.76863 (2020).
71. Johns, T. G. & Bernard, C. C. The structure and function of myelin oligodendrocyte glycoprotein. *J. Neurochem.* **72**, 1–9. https://doi.org/10.1046/j.1471-4159.1999.0720001.x (1999).
72. Bernard, C. C. et al. Myelin oligodendrocyte glycoprotein: a novel candidate autoantigen in multiple sclerosis. *J. Mol. Med. (Berl)* **75**, 77–88. https://doi.org/10.1007/s001090050092 (1997).
73. Nho, K. et al. Altered bile acid profile in mild cognitive impairment and Alzheimer's disease: Relationship to neuroimaging and CSF biomarkers. *Alzheimers Dement* **15**, 232–244. https://doi.org/10.1016/j.jalz.2018.08.012 (2019).
74. DeMorrow, S. Bile acids in hepatic encephalopathy. *J. Clin. Exp. Hepatol.* **9**, 117–124. https://doi.org/10.1016/j.jceh.2018.04.011 (2019).
75. Yang, Y., Eguchi, A., Mori, C. & Hashimoto, K. Depression-like phenotypes in mice following common bile duct ligation: Insights into the gut-liver-brain axis via the vagus nerve. *Neurobiol. Dis.* **192**, 106433. https://doi.org/10.1016/j.nbd.2024.106433 (2024).
76. Zorova, L. D. et al. Mitochondrial membrane potential. *Anal. Biochem.* **552**, 50–59. https://doi.org/10.1016/j.ab.2017.07.009 (2018).
77. Sokol, R. J. et al. Role of oxidant stress in the permeability transition induced in rat hepatic mitochondria by hydrophobic bile acids. *Pediatr. Res.* **49**, 519–531. https://doi.org/10.1203/00006450-200104000-00014 (2001).
78. Cheng, C., Yang, C., Jia, C. & Wang, Q. The role of cerebellum in Alzheimer's disease: A forgotten research corner. *J. Alzheimers Dis.* **95**, 75–78. https://doi.org/10.3233/JAD-230381 (2023).
79. Yang, C., Liu, G., Chen, X. & Le, W. Cerebellum in Alzheimer's disease and other neurodegenerative diseases: an emerging research frontier. *MedComm* **5**(7), e638. https://doi.org/10.1002/mco2.638 (2024).
80. Jalil, A. et al. Bile acid 7alpha-dehydroxylating bacteria accelerate injury-induced mucosal healing in the colon. *EMBO Mol. Med.* https://doi.org/10.1038/s44321-025-00202-w (2025).

Acknowledgements

We thank the Metabolomics and Lipidomics team at the Faculty of Biology and Medicine, University of Lausanne for the bile acid analysis.

Author contributions

OB: conceptualization, funding acquisition, interpretation of the histological and biochemical data, drafting and reviewing of the manuscript. VM: conceptualization, funding acquisition, interpretation of the data, drafting and reviewing of the manuscript. DS: performed BDL surgery, follow-up of the animals and sample collection, performed histological measures, final approval of the version to be published. KP: conceived and designed the study, funding acquisition, designed histological measures, analyzed and interpreted histological and biochemical data, statistical analysis, creation of the first draft of the manuscript and final version, project administration

and supervision.

Funding
The authors declare that financial support was received for the research, authorship, and/or publication of this article. K.P. was supported by the CIBM Center for Biomedical Imaging of the University of Lausanne (UNIL), University of Geneva (UNIGE), Geneva University Hospitals (HUG), Lausanne University Hospital (CHUV), and the École Polytechnique Fédérale de Lausanne (EPFL), as well as by the Leenaards and Jeantet Foundations. Additional funding was provided by the Swiss National Science Foundation (SNSF, project no. 310030_201218) and the EPFL (Fonds enseignement et recherche, project no. 22320).

Declarations

Competing interests
The authors declare no competing interests.

Additional information
Supplementary Information The online version contains supplementary material available at https://doi.org/10.1038/s41598-025-21054-x.

Correspondence and requests for materials should be addressed to K.P.

Reprints and permissions information is available at www.nature.com/reprints.

Publisher's note Springer Nature remains neutral with regard to jurisdictional claims in published maps and institutional affiliations.